

Multiscale Higher Order TV Operators for ℓ_1 Regularization and Their Relationship to Daubechies Wavelets

Toby Sanders and Rodrigo B. Platte

School of Mathematical and Statistical Sciences, Arizona State University, Tempe, AZ, USA.

Abstract

In the realm of signal and image denoising and reconstruction, ℓ_1 regularization techniques have generated a great deal of attention with a multitude of variants. A key component for their success is that under certain assumptions, the solution of minimum ℓ_1 norm is a good approximation to the solution of minimum ℓ_0 norm. In this work, we demonstrate that this approximation can result in artifacts that are inconsistent with desired sparsity promoting ℓ_0 properties, resulting in subpar results in some instances. With this as our motivation, we develop a multiscale higher order total variation (MHOTV) approach, which we show is closely related to the use of multiscale Daubechies wavelets. In the development of MHOTV, we confront a number of computational issues, and show how they can be circumvented in a mathematically elegant way, via operator decomposition and alternatively converting the problem into Fourier space. The relationship with wavelets, which we believe has generally gone unrecognized, is shown to hold in several numerical results, although subtle improvements in the results can be seen due to the properties of MHOTV.

1 Introduction

Since its formal introduction in 1992 [27], total variation (TV) denoising has become a very popular method for signal denoising, as well as signal reconstruction problems. Along with TV, a large variety of approaches for similar ℓ_1 regularization approaches have also been proposed for an array of problems [17, 19, 33, 6, 9]. Signal and image recovery methods continue to attract a great deal of interest due to the wide variety of potential applications and ever increasing means of various sensing mechanisms to acquire data. To name a few, synthetic aperture radar (SAR), magnetic resonance imaging (MRI), electron tomography, and inpainting are all image recovery applications that have advanced in part due to ℓ_1 regularization methods [20, 1, 23, 24, 4, 40, 22], and in each case the approach can be tailored to the challenges that the particular application poses. For example, in SAR, although a large data set is often acquired from which the image can be reconstructed, this data often comes with imperfections and the pixelated images reconstructed take on complex values with phase values that vary randomly. With many problems such as MRI and electron

tomography, the challenge is often to acquire as little data as necessary due to possible damage of the subject being imaged or because of time constraints, thus requiring the need for inverse methods that can achieve the absolute best results.

The mathematical description of the general problem we are interested is to recover a signal or image $f \in \mathbb{R}^N$, from noisy measurements b of the form $b = Af$, where $A \in \mathbb{R}^{m \times N}$ is some sensing matrix that approximates the physical model of the particular problem. Then the ℓ_1 regularized solution is given by

$$f_{rec} = \arg \min_f \left\{ \|Af - b\|_2^2 + \lambda \|Tf\|_1 \right\}, \quad (1)$$

where T is some sparsifying linear transform and λ is a parameter that balances the effects of the data and regularization terms. The feasibility of this approach is that some a priori knowledge of the signal suggests that Tf is sparse, and that the formulation with the ℓ_1 norm encourages such sparsity [14, 7, 8]. In many applications, knowledge of the “right” transform is roughly available, particularly with images and for other signals as well, this knowledge is in the form of some “smoothness.”

In the case of TV, the sparsifying transform is given by $T : \mathbb{R}^N \rightarrow \mathbb{R}^{N-1}$, where $(Tf)_i = f_{i+1} - f_i$. The general idea for this approach is that the signal f is assumed to be piecewise constant with a few “boundary” points, in which case Tf is sparse. If this is not precisely true, this approach still effectively reduces unwanted oscillations at the cost of the well documented stair-casing effect [9, 5]. However, for more general piecewise smooth functions higher order TV (HOTV) methods can be more effective [9, 6]. In this case the transform maps f to higher order finite differences of f , whereas the TV transform can be considered a first order finite difference.

Another very popular choice for T are wavelet transforms. For instance, such a transform can be written as $T : \mathbb{R}^N \rightarrow \mathbb{R}^N$, where $(Tf)_j = \langle f, \psi_j \rangle$ and ψ_j are orthonormal so that $f = \sum_j \langle f, \psi_j \rangle \psi_j$. The idea here is that for appropriately smooth signals, most of the signal’s energy is captured in the few low frequency, larger scaled elements of the basis. Thus very few of the high frequency, small support basis coefficients (of which occupy the majority number of the basis elements) are nonzero, and thus a sparse representation of f exists with respect to the basis.

2 Discussion and Contribution

Perhaps the primary motivating application driving the development of wavelets in the early 90’s was fast and effective signal, image, and video compression and denoising, which led to an elegant theory of sparse representation of signals through multiresolutional basis functions [13, 38]. The development also led to numerous fast wavelet transforms [3, 2, 10] and multidimensional generalizations, such as curvelets and shearlets [17, 19, 32]. One of the most important properties of wavelets are the orthogonality conditions, or in the case of a redundant system are the tight frame conditions. These properties are fundamental to compression and soft wavelet thresholding methods [15, 36], as the compression rate can be measured directly through the change in the ℓ_2 norm of the coefficients by Parseval’s theorem.

It is well established that ℓ_1 regularization techniques can take advantage of a wavelet basis to promote sparsity for image reconstruction. Perhaps less known is that one does not need to be concerned with *all* of the coefficients of a wavelet basis, but really only the high frequency wavelets. Indeed, the transforms associated with approaches such as TV and HOTV are only concerned with highly localized analysis of the function behavior. In addition, the orthogonality conditions of wavelets that are fundamental to compression and denoising may not be necessary for ℓ_1 regularization techniques and may serve as an unnecessary limiting constraint.

Although not a regularly discussed fact, TV has been shown equivalent (somewhat a trivial fact) to soft thresholding with the highest frequency basis functions of the Haar wavelets [34, 35], thus not a far cry from wavelet methods. The main difference between such methods is that TV and other similar transforms concern only with the local scale, whereas wavelets methods consider smoothness at all scales. However, it is our intuition that we should be considering something between these two extremes.

The crux of these methods was in that recovering a signal with the most sparse representation, i.e. the smallest so called ℓ_0 norm, is often equivalent to its convexly relaxed variant, which recovers the signal with the smallest ℓ_1 norm. This equivalence has its own devoted field called compressed sensing (CS) [14, 7, 8]. Although convex ℓ_1 optimization algorithms are useful in promoting sparsity, unfortunately some “small” coefficients may still linger, an obvious sign that the exactness guarantees given by CS theory sometimes do not hold in practice.

In this paper, we develop an alternative method for TV and HOTV methods which we refer to as multiscale HOTV (MHOTV). The motivation for such an approach is in observable sub par results due to the relaxation of the sparsity promotion through the ℓ_1 norm, which we determined calls for analysis of the function behavior at multiple scales. Hence we develop a multiscale version of these transformations. As can be immediately deduced, this multiscale strategy is similar to the treatment of wavelets, and we argue that our approach is in fact closely related to the use of Daubechies wavelets, with the main divergence coming in the orthogonality condition prescribed by the wavelets. Orthogonality may be unnecessary for ℓ_1 regularization techniques, and the relaxation of this condition in our approach allows for better localization of the transform. In the development of MHOTV, we carefully tackle the computational concerns associated with our approach through the use of both the FFT and operator decompositions. We are able to show through several numerical examples that MHOTV provides an improvement to the current alternatives.

The organization of the remainder of the paper is as follows. In section 3 we define the HOTV operators and the corresponding multiscale generalizations. We also motivate the approach via a numerical example, and make the connection with Daubechies wavelets. In section 4 we precisely define the MHOTV ℓ_1 regularization model and give precise normalizations to deal with proper parameter selection. In section 4.1 we address the computational concerns associated with calculating MHOTV coefficients, devising two distinct ways that they can be calculated in an efficient manner. In section 5 we provide numerical results for 1-D and 2-D reconstruction problems, showing that MHOTV is an improvement to the original HOTV and the related Daubechies wavelets. Some proofs and definitions are provided in the appendix.

3 HOTV and Multiscale Generalizations

As an alternative to TV regularization, general order TV methods have been shown to be effective for ℓ_1 regularization [9, 6, 31, 1]. The TV transform can be thought of as a finite difference approximation of the first derivative, thus annihilating a function in locations where the function is a constant, i.e. a polynomial of degree zero. Likewise, higher order TV transforms can be considered higher order finite difference approximations to higher order derivatives, thus annihilating the corresponding degree polynomials. With this in mind, we have the following definition:

Definition 1 (Finite Differences). *Let $\phi_k \in \mathbb{R}^N$ be defined by*

$$(\phi_k)_j = \begin{cases} (-1)^{k+j-1} \binom{k}{j-1} & \text{if } 1 \leq j \leq k+1 \\ 0 & \text{if } k+1 < j \leq N \end{cases}. \quad (2)$$

Then for $f \in \mathbb{R}^N$, the periodic k^{th} order finite difference of f is given by

$$f * \phi_k,$$

where $$ denotes the discrete convolution.*

Remark 1. *The convolution in this definition (and in general) can be represented by multiplication with a circulant matrix Φ_k , where each row of Φ_k holds a shifted version of ϕ_k . An example of the matrix in the case $k = 2$ is given in (3). Note that this definition uses a periodic extension of f and can be ignored by dropping the last k rows of Φ_k .*

$$\Phi_2 = \begin{pmatrix} 1 & -2 & 1 & 0 & \dots & 0 \\ 0 & 1 & -2 & 1 & \dots & 0 \\ 0 & 0 & 1 & -2 & \dots & 0 \\ \vdots & & \ddots & & \dots & \vdots \\ 1 & 0 & \dots & & 1 & -2 \\ -2 & 1 & \dots & & 0 & 1 \end{pmatrix}. \quad (3)$$

With this definition, the HOTV model can be said to recover

$$f_{\text{rec}} = \arg \min_f \left\{ \|Af - b\|_2^2 + \lambda \|\Phi_k f\|_1 \right\}. \quad (4)$$

Unfortunately for many real world imaging problems the equivalence between ℓ_1 and ℓ_0 may not hold in practice, yet the ℓ_1 regularization still tends to encourage favorable solutions. In terms of the sparsity promoting transform, this means that the transform of the recovered function may not be truly sparse, but most of the values are instead relatively close to zero. For HOTV, this means that a local Taylor expansion of the recovered function will still contain some small nonzero higher order coefficients, yet essentially unobservable at the very local scale. In other words, at some point t , there exists a polynomial expansion of minimal degree of f given by

$$f(x) \approx \sum_{j=0}^M \alpha_j(t) \frac{(x-t)^j}{j!}, \quad (5)$$

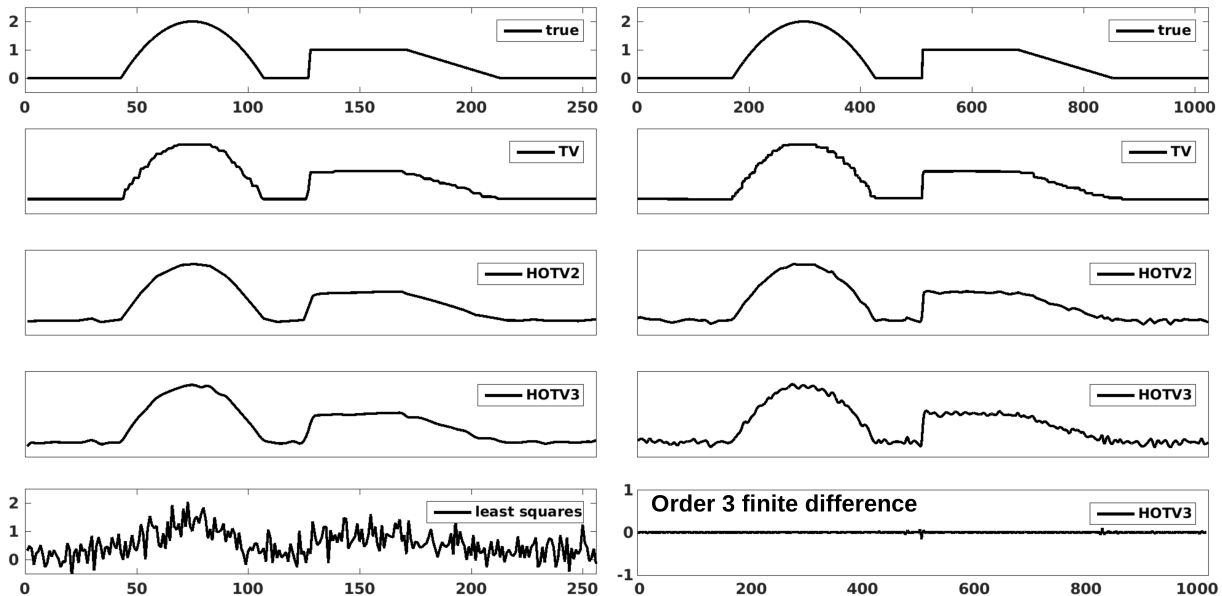


Figure 1: The top four rows present the reconstruction of a piecewise polynomial function of degree two over 256 (left column) and 1024 (right column) points from random sampling at 50%. The corresponding least squares solution is shown in the bottom left, and the 3rd order finite difference of the HOTV3 solution over the 1024 grid is shown on the bottom right.

which holds for all x within some small interval I around the point t . Ideally a solution given by the order k HOTV model recovers a solution so that the coefficients $\alpha_j(t)$ vanish for $j \geq k$. The ℓ_1 model allows for these coefficients to remain, although very small, and the function still *appears* to essentially be a polynomial of degree less than k . However, when this behavior persists over many points at a larger scale, the result can be a function which looks more like a trigonometric polynomial rather than an algebraic one.

This phenomenon is demonstrated in Figure 1, where a piecewise polynomial of degree two was reconstructed from random noisy samples with 50% sampling¹ using TV and HOTV regularizations. The sampling matrix $A \in \mathbb{R}^{N/2 \times N}$ is constructed so that a random 10% of its entries are set to be nonzero, where these nonzero values are uniformly distributed over $[0, 1]$. The samples were corrupted with normally distributed mean zero noise. Two different grid sizes are demonstrated, 256 and 1024, and it can be observed that these small oscillations become increasingly abundant with more grid points. However, in the bottom of the figure, the third order finite difference of the HOTV3 solution shows that locally this oscillatory behavior results in almost exact low order polynomials, although *very* small amplitudes persist in the transformed domain and thus not truly sparse in the ℓ_0 sense. Nevertheless, all regularization approaches should still be deemed useful, as evidenced by the least squares solution to the problem shown in the bottom left panel of the figure.

Due to this phenomena we propose a multiscale HOTV approach, which considers the regularization transform at multiple scales. The idea is that a larger stencil would recognize

¹The number of samples is half the number of grid points.

these oscillations even with the ℓ_1 norm. As TV generalizes to the Haar wavelet by stretching and scaling of the elements, we propose the same with HOTV. To this end we give the following definition.

Definition 2 (Multiscale Finite Differences). *Let $\phi_{k,m} \in \mathbb{R}^N$ be defined by*

$$(\phi_{k,m})_j = \begin{cases} (-1)^{k+\lceil \frac{j}{m} \rceil - 1} \binom{k}{\lceil \frac{j}{m} \rceil - 1} & \text{if } 1 \leq j \leq m(k+1) \\ 0 & \text{if } m(k+1) < j \leq N \end{cases}. \quad (6)$$

Then for $f \in \mathbb{R}^N$, the periodic k^{th} order finite difference of scale m of f is given by

$$f * \phi_{k,m},$$

where $$ denotes the discrete convolution.*

Remark 2. *Again, this convolution can be represented as multiplication with a circulant matrix $\Phi_{k,m}$. An example of $\Phi_{k,m}$ in the case $k=2$ and $m=2$ is given in (7).*

$$\Phi_{2,2} = \begin{pmatrix} 1 & 1 & -2 & -2 & 1 & 1 & 0 & \dots & 0 \\ 0 & 1 & 1 & -2 & -2 & 1 & 1 & \dots & 0 \\ 0 & 0 & 1 & 1 & -2 & -2 & 1 & \dots & 0 \\ \vdots & & & \ddots & & & & \dots & \vdots \\ -2 & -2 & 1 & 1 & 0 & 0 & \dots & 1 & 1 \\ 1 & -2 & -2 & 1 & 1 & 0 & \dots & 0 & 1 \end{pmatrix}. \quad (7)$$

3.1 Relationship to Daubechies Wavelets

Wavelets are first characterized by the following properties [12, 25]:

1. They are generated by a multiresolutional analysis.
2. They form an orthonormal basis, or in the case of a redundant system, they typically form a tight frame.

From these two characteristics, there are a number of flexibilities in the design of the wavelets, which can be suited towards the particular application. The most common, is given by the smoothness and localization properties of the wavelets. For Daubechies wavelets the smoothness is characterized by the number of vanishing moments, i.e. the polynomial of maximal degree to which the wavelet is orthogonal. With this design, low order polynomial exhibit a sparse representation in the basis representation.

To develop a basic mathematical formulation of wavelet expansion, let us suppose we would like a orthonormal wavelet basis for a subset of functions on $L_2[0, 1]$. In the interest of digitization, let's take the space of functions to be *uniform pixelated* functions of the form

$$f(x) = \sum_{j=0}^{N-1} c_j \mathbb{1}_{I_j}(x), \quad \text{where } I_j = \left[\frac{j}{N}, \frac{j+1}{N} \right). \quad (8)$$

For simplicity, we take $N = 2^n$. For this space of functions, if we denote our scaling function by φ and the mother wavelet by ψ with $\text{supp } \varphi = \text{supp } \psi = [0, 1]$, then we have the following orthonormal wavelet expansion

$$f = \sum_{k=0}^{2^p-1} \langle f, \varphi_{p,k} \rangle \varphi_{p,k} + \sum_{j=p}^{n-1} \sum_{k=0}^{2^j-1} \langle f, \psi_{j,k} \rangle \psi_{j,k}. \quad (9)$$

Here,

$$\psi_{j,k}(x) = 2^{j/2} \psi \left(2^j x - \frac{k}{2^n} \right) \quad \text{and} \quad \varphi_{j,k}(x) = 2^{j/2} \varphi \left(2^j x - \frac{k}{2^n} \right),$$

i.e. shrinking and scaling of the of the generating wavelet functions, where higher values of j correspond to the more localized elements of the expansion. The value p is an positive integer with $0 \leq p \leq n$, and the value $n - p$ is said to be the number of *scales* in the wavelet expansion². With the representation in (9), the coefficients for the scaling functions in the first sum capture most of the energy of the signal, and the wavelet coefficients *vanish* at points where f is a polynomial (discretized) of sufficiently low degree according to the number of *vanishing moments* prescribed for the wavelets.

As a trade off, an increasing number of vanishing moments chosen for the wavelet basis results in an increase in the support of the wavelet functions. Daubechies wavelets are designed to yield the orthonormal wavelet basis of minimal support given a selected number of vanishing moments [25].

Connecting these ideas to HOTV, we see that these transforms are playing similar roles. Indeed, both are prescribed by the number of vanishing moments, or in the language of HOTV, the highest order polynomial that is annihilated by the approach. Furthermore, both are designed to yield minimal support given the number of vanishing moments. The crucial difference lies in the orthogonality condition prescribed by wavelets, which further increases the support of the wavelet elements. We emphasize again, that this condition is fundamental to compression and threshold denoising methods, but not necessarily useful with general image reconstruction problems.

For ℓ_1 regularization, we only need to be concerned with regularization of the wavelet coefficients in (9), and thus the coefficients for the scaling functions in the first sum can be removed in the regularization. Finally, one additional wrinkle used for ℓ_1 regularization (and denoising as well) implementation the use a wavelet frame by simply taken all possible shifts for each scaling of the wavelets, which is sometimes referred to as translational invariant cycle spinning [11, 37, 18]. This eliminates the lack of translation invariance of a wavelet basis that can otherwise result in unwanted artifacts near discontinuities. The case when $p = n - 1$ would be most closely related to the original HOTV, which is when only the elements at the finest scale are used. However, for smaller values of p the wavelets are more comparable to the MHOTV development in this paper.

²For $p = n$ it is understood that the second sum is removed.

4 MHOTV Reconstruction Model

We now present the general model for MHOTV reconstruction. Generally speaking, we still use the model presented in (1), where A maps the unknown function f to some perhaps noisy measurements given by b , from which we use to reconstruct f . Our sparsity promoting transforms are now given by the matrices $\Phi_{k,2^m}$, for $m = 0, 1, \dots, \ell$, where ℓ is the maximum scaling of the operator used and k is the chosen order. Setting our maximum scaling to $\ell = 0$ corresponds to the traditional HOTV approach. Although not completely necessary, we choose a dyadic scaling of the operators, similar to the treatment of wavelets. As with wavelets, we will show that this is convenient for computational purposes. Finally then our reconstruction model is given by

$$f_{rec} = \arg \min_f \left\{ \|Af - b\|_2^2 + \frac{\lambda}{\ell + 1} \sum_{m=0}^{\ell} 2^{-m} \|\Phi_{k,2^m} f\|_1 \right\}. \quad (10)$$

The factor of 2^{-m} is a normalization that accounts for the increasing norms of each operator, which would otherwise weigh too heavily to the largest scaling operator. The scaling of the parameter λ by $\ell + 1$ simplifies the selection of the parameter, which would otherwise need to be manually scaled by such a factor to account for the number of scales being used. An additional scaling of λ can be used to account for the order k of the method as well [30].

Calculation of traditional HOTV coefficients is a computationally inexpensive task, due to the sparsity of the matrix operator. However, with increasing dyadic scales the direct calculation increases exponentially. Due to this, in the proceeding section we develop two distinct approaches that show that these calculations can be carried out with linear increase in the flop count with respect to the number of scales used.

4.1 Fast Calculation of MHOTV Operators

Fast computation of standard HOTV can be done in several ways. One can construct the sparse matrix Φ_k and perform matrix computations directly, a calculation with runtime of kN flops. One could make use of other procedures, such as MATLAB's "diff" command which requires the same flop count without storing the matrix. With MHOTV, these approaches become less appealing. With matrix construction, if one is using several scales, then several matrices need to be computed and stored, and the matrices become significantly less sparse for larger scales. The "diff" command cannot be implemented directly for larger scale HOTV operators.

Another alternative is to use the Fourier convolution theorem to perform the convolution operation via a product in Fourier space. For the traditional HOTV operators, this can be fairly slow compared with the matrix and "diff" approach, since the necessary two discrete Fourier transforms would require $\sim 2N \log_2 N$ flops compared with the kN flops for the alternative implementations. However, this method is relatively comparable for MHOTV, since the Fourier transforms only need to be computed once to determine the coefficients at all scales.

We outline two procedures for efficient calculation of MHOTV. First, we describe the Fourier approach, where we derive precise formulas for the MHOTV Fourier filters. Sec-

ond, we describe an alternative efficient approach by decomposition of the MHOTV matrix operators.

4.1.1 Computation via Fourier Transforms

By the Fourier convolution theorem, the MHOTV operators can be computed as multiplications in Fourier space, i.e.

$$f * \phi_{k,m} = F^{-1}(F(f) \cdot F(\phi_{k,m})), \quad (11)$$

where F denotes the discrete Fourier transform. Although this can be numerically computed, it is a nice theoretical result to have an exact formula for the discrete Fourier transform of $\phi_{k,m}$. Moreover, analytic determination of $F(\phi_{k,m})$ allows us to generalize the MHOTV to fractional orders.

Proposition 1. *The DFT of the vector $\phi_{k,m}$ defined in (6) has an explicit expression given by*

$$F(\phi_{k,m})_\xi = \frac{\left(e^{\frac{-i2\pi\xi m}{N}} - 1\right)^{k+1}}{e^{\frac{-i2\pi\xi}{N}} - 1}, \quad (12)$$

for $\xi = 0, 1, \dots, N-1$.

Proof. The expression for the ξ^{th} Fourier coefficient in the DFT of $\phi_{k,m}$ is given by

$$F(\phi_{k,m})_\xi = \sum_{n=1}^N (\phi_{k,m})_n e^{\frac{-i2\pi\xi}{N}(n-1)}. \quad (13)$$

Notice that the terms $n > m(k+1)$ vanish by definition of $\phi_{k,m}$. For the smaller terms, notice that the values of $\phi_{k,m}$ repeat over strings of length m . Therefore each of these corresponding strings of trigonometric terms in (13) get the same weights, leading to the following sum:

$$F(\phi_{k,m})_\xi = \sum_{j=0}^k \left((-1)^{j+k} \binom{k}{j} \left[\sum_{\ell=0}^{m-1} e^{\frac{-i2\pi\xi}{N}(jm+\ell)} \right] \right). \quad (14)$$

Here the inner sum represents the m consecutive terms in (13) that receive the same weights from $\phi_{k,m}$, namely $(-1)^{j+k} \binom{k}{j}$. Switching the order of summation, we recognize the sum over j as a binomial expansion leading to

$$\begin{aligned} F(\phi_{k,m})_\xi &= \sum_{\ell=0}^{m-1} \sum_{j=0}^k (-1)^{j+k} \binom{k}{j} e^{\frac{-i2\pi\xi}{N}(jm+\ell)} \\ &= \sum_{\ell=0}^{m-1} \left(e^{\frac{-i2\pi\xi}{N}m} - 1 \right)^k e^{\frac{-i2\pi\xi}{N}\ell}. \end{aligned}$$

The remainder of the proof follows by elementary calculations. □

4.1.2 Fast Computation via Operator Decomposition

In this section, we give a decomposition for the matrix operator $\Phi_{k,2^m}$ and describe how this decomposition can be used for rapid calculation of MHOTV operators. The decomposition of $\Phi_{k,2^m}$ is given in the following theorem.

Theorem 1. *Let the matrix P_m with entries $\{p_{i,j}\}_{i,j=1}^N$ be defined by*

$$p_{i,j} = \begin{cases} 1 & \text{if } j = i \\ 1 & \text{if } j = (i + m - 1) \bmod (N) + 1 \\ 0 & \text{if otherwise} \end{cases} \quad (15)$$

Then the following holds:

1. *The entries of P_m^{k+1} , which we denote by $\{p_{i,j}(m, k)\}_{i,j=1}^N$, are given by*

$$p_{i,j}(m, k) = \begin{cases} \binom{k+1}{\ell} & \text{if } j = (i + m\ell - 1) \bmod (N) + 1 \\ 0 & \text{if otherwise} \end{cases},$$

where it is implied ℓ is an integer satisfying $0 \leq \ell \leq k + 1$.

2. *$\Phi_{k,2^m}$ has the decomposition*

$$\Phi_{k,2^m} = P_m^{k+1} P_{m-1}^{k+1} \cdots P_1^{k+1} \Phi_k \quad (16)$$

and therefore

$$\Phi_{k,2^m} = P_m^{k+1} \Phi_{k,2^{m-1}}. \quad (17)$$

3. *The equality in (16) holds for any rearrangement of the product of matrices.*

The proof of this theorem is given in the appendix. The matrices P_2 and P_2^2 are shown below to illustrate the sparse structure of these operators:

$$P_2 = \begin{pmatrix} 1 & 0 & 1 & 0 & \cdots & 0 \\ 0 & 1 & 0 & 1 & \cdots & 0 \\ \vdots & & \ddots & & \cdots & \vdots \\ 0 & 1 & 0 & \cdots & & 1 \end{pmatrix}, \quad P_2^2 = \begin{pmatrix} 1 & 0 & 2 & 0 & 1 & \cdots & 0 \\ 0 & 1 & 0 & 2 & 0 & \cdots & 0 \\ \vdots & & \ddots & & & \cdots & \vdots \\ 0 & 2 & 0 & 1 & 0 & \cdots & 1 \end{pmatrix}. \quad (18)$$

Proposition 2. *Direct calculation of $\Phi_{k,2^m}$ requires $2^m Nk$ flops. The same calculation using the decomposition in (16) requires $mN(k+1) + Nk$ flops. The same calculation using the Fourier method requires $2N \log_2 N + N$.*

Proposition 2 is a direct result of Theorem 1, the Fourier convolution theorem combined with the FFT, and the flops required for the direct calculation. We assume that the FFT and inverse FFT can be computed in $N \log_2 N$ flops, although the exact count is somewhat vague, depending on the precise algorithm and if N is a power of 2. A few concluding remarks are in order.

Remark 3. When concerned with solving (10), if we use the decomposition approach to calculate the operators as determined by (16), the associated computations are limited to that at the highest scale, since the intermediate scales are determined in this calculation as pointed out in (17). Thus with $\ell + 1$ scales, then by Proposition 2 the total flop count for computing all $\ell + 1$ scales is $\ell N(k + 1) + Nk$.

Remark 4. If we use the Fourier approach for calculating the coefficients in (10), only one forward FFT is required for the function f . Then the product of $F(f)$ and $F(\phi_{k,2^m})$ must be computed for each m , as well as the inverse FFT for each of these products. With $\ell + 1$ scales, this gives a flop total to $(\ell + 2)N \log_2 N + (\ell + 1)N$.

Remark 5. All of the results presented are for 1-D signals. For higher dimensions say 2-D, the operators can be applied along each row and column, and the flop count is only doubled, disregarding the likely increased number of indices.

Remark 6. To solve (10), we use the well established alternating direction method of multipliers (ADMM) [21, 16, 39]. This approach introduces splitting variables that allows one to split the objective functional into equivalent subproblems that can be solved relatively fast. Our algorithm can be downloaded at [28], and some of the simulations in the proceeding section can also be found there.

5 Numerical Experiments

5.1 Repeat of 1-D Simulations

To compare MHOTV and wavelet regularized reconstructions we repeat the numerical examples presented in Figure 1 with the same noisy data used for the HOTV reconstruction. The corresponding reconstruction with MHOTV and wavelets are presented in Figure 2. Recall that the measurements were collected at a 50% sampling rate and corrupted with normally distributed mean zero noise. For the multiscale HOTV and wavelets, three scaling levels were used. The selection of the regularization parameter λ was set to the same relative value for each order³ for HOTV and the wavelets, where we used a similar normalization approach for the wavelets coefficients as presented in (10).

The results in Figure 2 were generated with orders 1, 2, and 3. The order is indicated with the numbers next to the approach in the legends, e.g. we denote the order $k = 3$ MHOTV approach with MHOTV3. For a baseline comparison, the least squares solution is shown in the top right panel. Compared with the corresponding 1024 reconstructions from HOTV in Figure 1, these solutions show clear improvements, particularly with the higher orders. As we expect, although the MHOTV1 and Haar wavelet coefficients are computed in a very different manner, the resulting reconstruction are nearly identical since the models are theoretically equivalent. They both exhibit the staircasing and noise effects in precisely the same locations. The higher order approaches also show many similar effects of the noisy features, exhibiting certain oscillatory features with the same general behavior in precisely the same locations. However, with the higher orders, these approaches are not equivalent

³The parameter λ was appropriately rescaled for each order [30].

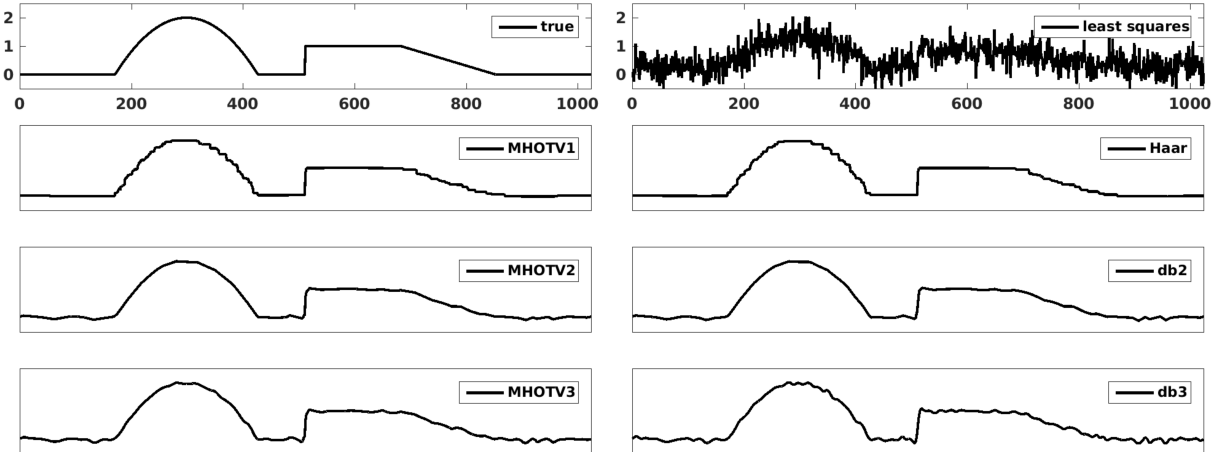


Figure 2: Reconstruction of a piecewise polynomial function of degree two over 1024 stencil from random sampling at 50%. Three scales are used for both the Daubechies wavelets and multiscale HOTV.

and MHOTV provides regulatory information at finer scales due to the minimal support of the transform elements. The result appears to be a modest improvement in the resulting reconstructions.

5.2 2-D Tomographic Simulations

In this section, we investigate the regularization methods on the common 2-D tomographic image reconstruction problem [26]. The phantom test image is shown in Figure 3 (a). The data generated for tomography are 1-D line integrals of the image, well-known as Radon transform data. Formally, the Radon transform of a 2-D function or image f is defined as

$$Rf(t, \theta) = \int_{\Omega} f(x, y) \delta(t - (x, y) \cdot (\cos \theta, \sin \theta)) dx dy, \quad (19)$$

where Ω is the image domain and δ is the Dirac delta function. As in many applications, the data collected for reconstruction are of the form known as parallel beam geometry. In this setting, the full knowledge of noisy $Rf(t, \theta)$ is known for some finite set of angles, θ .⁴ In this numerical experiment, we use a total of 29 angles that are equally distributed across the full 180° angular range, which are visualized as a sinogram in Figure 3 (b). Such a limited set of data is sometimes referred to as *limited data* tomography. Mean zero normally distributed noise was again added to the data values. Classically tomographic reconstruction from parallel beam geometry can be done by first transforming the data into Fourier space by the Fourier slice theorem, and then applying a chosen ramp filter to this data and the inverse Fourier transform. This direct approach, called filtered backprojection, is sensitive to noise and is shown in Figure 3 (c).

The problem can however be discretized and approximated by a set of linear equations $Af = b$ (see for instance [29] on pages 8-9 within section 1.5.), where A is sparse matrix that

⁴There is also a discretization over t , but it is small enough to ignore.

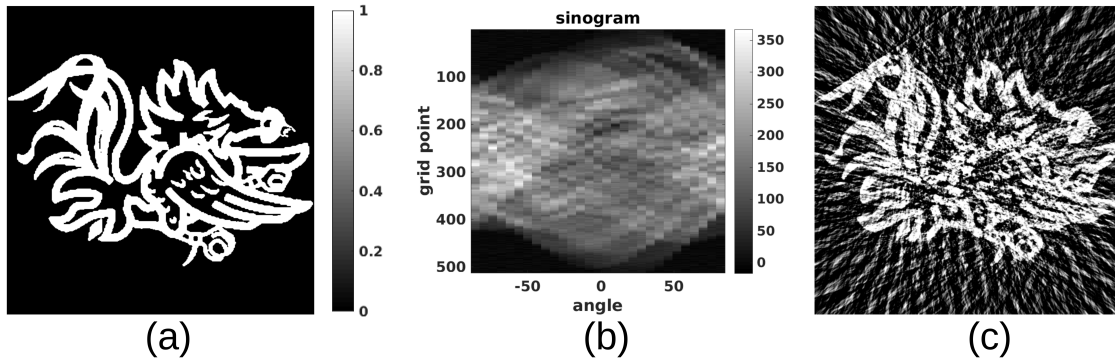


Figure 3: (a) Phantom image. (b) Noisy tomographic data in sinogram format, 29 projections in total. (c) Classical filtered backprojection reconstruction from data.

is a discretized approximation of the Radon transform, f is the vectorized image, and b is a vector holding the data values. With this set up we can apply regularization models such as (1) and (10). We use a 512×512 pixelated mesh for the image domain in this experiment. The results for applying these models with HOTV, MHOTV, and Daubechies wavelets all at orders one and three are shown in Figure 4. Each of the models are also supplemented with a nonnegativity constraint, $f \geq 0$, which is carried out with a projected gradient method. A baseline comparison obtained by a conjugate gradient least squares solver is also shown in the figure. To ensure accurate comparison between the methods by appropriate parameter selection and algorithmic convergence, the relative data errors defined by $\|Af - b\|_2 / \|b\|_2$ are shown in the figure, and it confirms that each approach approximately fit the data equally well, with all of the errors contained within an interval of size 0.0129.

As has been observed previously [31], due to a number of reasons including undersampling, noise, fine details between the image features, and nature of the regularization, the order 1 solutions (TV) can leave the fine features under resolved, even though the underlying image is truly a piecewise constant that classical TV was originally designed to recover. Each of these order 1 images appear relatively similar, with the MHOTV and Daubechies approaches showing modest improvements in resolving some features. As in the 1-D case, the HOTV3 solution exhibits some small local oscillations that appear as noise in the image. However, this image, as well as the other order 3 approaches resolve the features notably more clear than the order 1 approaches. Both of the order 3 multiscale approaches appear less noisy than the HOTV order 3, while still maintaining a good approximation of the image features.

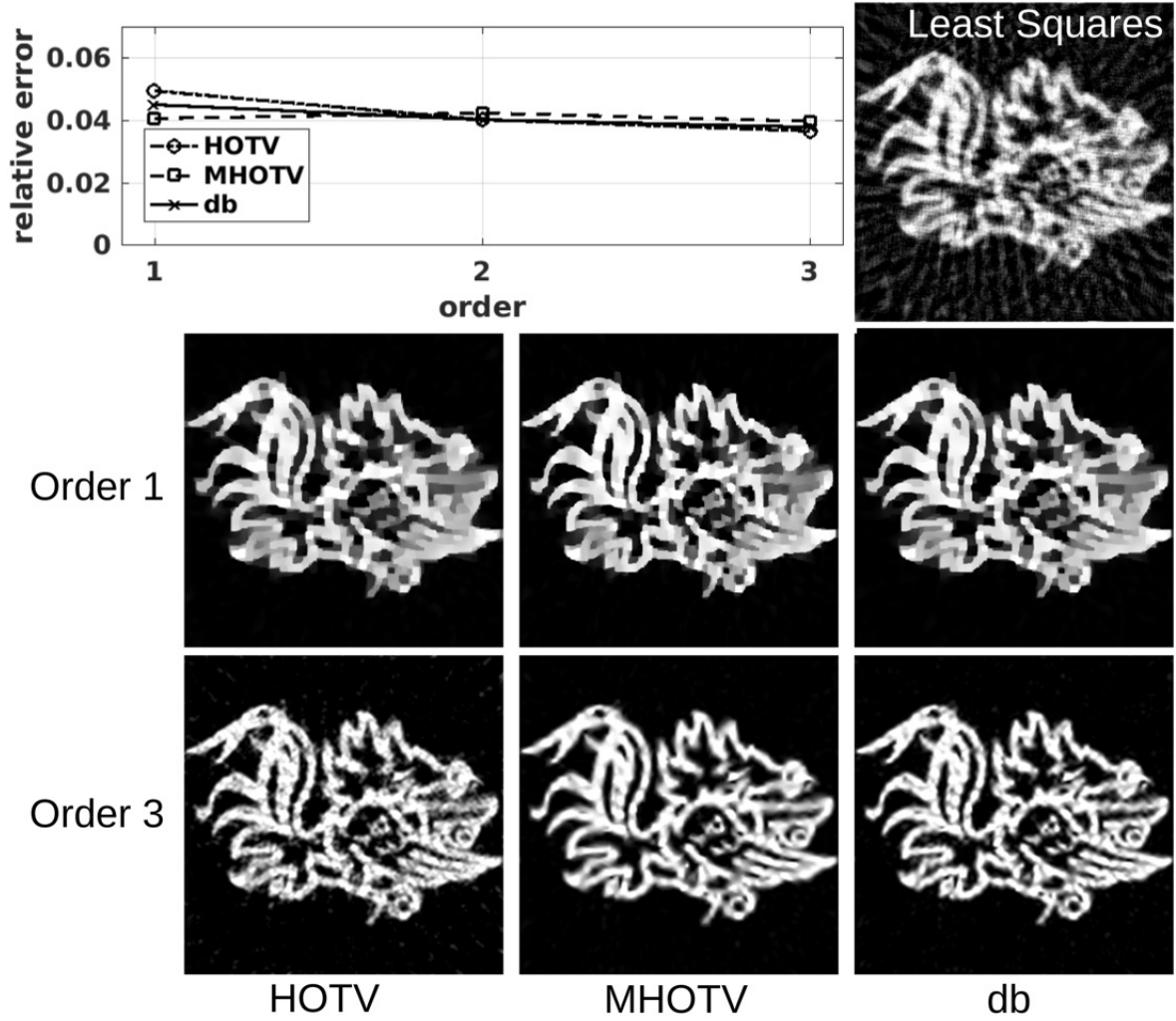


Figure 4: Reconstructions of phantom image from 29 tomographic projections. Orders 1 and 3 are shown for the regularization approaches. Top left: relative data fitting error from each approach shows approximately equivalent data fitting from each approach. Top right: least squares solution for baseline comparison.

5.3 Recovery Rates from Under-sampled Data

To compare the methods in a more quantitative manner, we run a series of numerical simulations and measure the rate of successful recovery for each method as a function of the sampling rate. The procedure is carried out in the following manner. For each simulation we randomly generate a piecewise polynomial of specified maximal degree over a 1024 stencil. This function is then randomly sampled at the specified sampling rate precisely as in the previous 1-D simulations, where the sampling rate is defined by the number of samples divided by the number of grid points, and here it takes on values less than 1. Each regularization procedure was then used for reconstruction, and the ℓ_2 error between the true function and reconstructed functions is determined. If the error was less than 10^{-2} , then the reconstruction was said to yield a *successful recovery*. This simulation was carried out for each sampling rate in 20 trials, and the fraction of those 20 trials that yielded successful recovery is set as our probability of success. In each case, the generated test functions had five discontinuities, and the location of the jumps were drawn randomly from a uniform distribution on the approximation interval.

No noise was added for these simulations, as this can make the likelihood of an exact recovery highly unlikely. Therefore, for this case our general ℓ_1 model as a modification of (1) is given by

$$f_{rec} = \arg \min_f \|Tf\|_1 \quad \text{s.t.} \quad Af = b, \quad (20)$$

and similarly for our specific MHOTV model in (10). This exact data fitting model is approximately solved by modifying the original algorithm with an additional Lagrangian multiplier for the data fitting term.

The results for these simulations are shown in Figure 5. The results are separated in two ways, by the degree of the piecewise polynomial function that is sampled (varying along the rows) and the order of the regularization method (varying along the columns). In the first row are results for piecewise constant functions, in the second row are piecewise linear functions, and in the third row are piecewise quadratic functions. In all cases, the MHOTV yields the highest probability of success, regardless of the degree of the polynomial or order of the regularization, and the Daubechies wavelets success appears to generally lie somewhere between MHOTV and HOTV. The order 1 regularizations perform well only in the case of piecewise constant functions. On the other hand, the order 2 and 3 regularizations perform well for all function types.

6 Summary

HOTV circumvents the staircasing often observed in TV solutions and has been shown to be more effective for problems with fine features, where resolution can be improved by increasing the order of derivatives in the regularization term [31]. In some applications, however, high order derivatives promote solutions with spurious local oscillations, as shown in Figure 1. The MHOTV regularization we introduce in this work is shown to mitigate unwanted oscillations while maintaining the resolution power of high order regularization.

Although the theory for MHOTV reconstructions remains underdeveloped when compared to wavelets regularization [13, 38, 17, 19, 32, 15, 36], our experiments indicate that

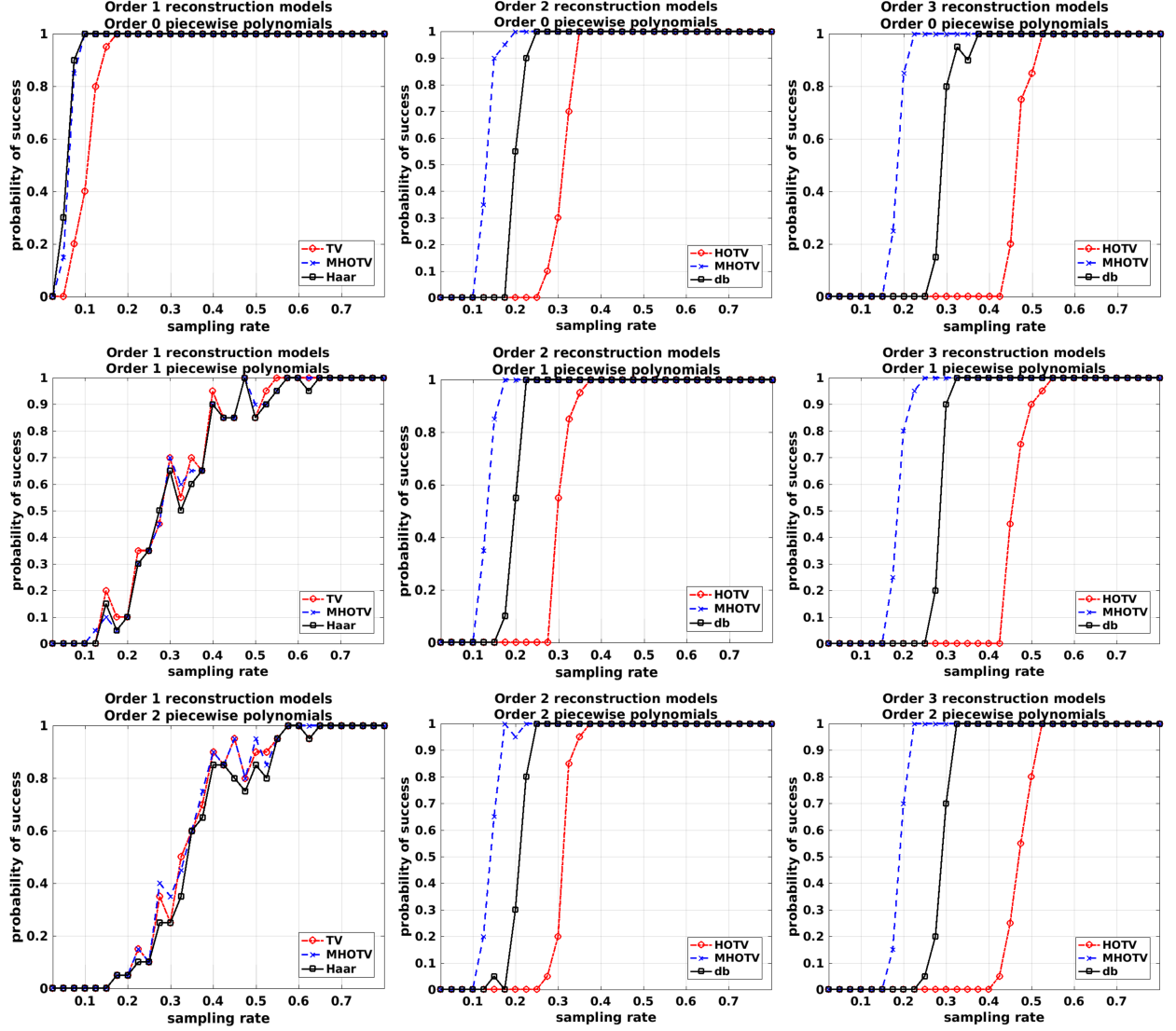


Figure 5: Probability of success for HOTV, MHOTV, and Daubechies wavelets at orders 1 (left column), 2 (middle column) and 3 (right column). A successful recovery is deemed whenever the relative ℓ_2 error between the reconstruction and the true signal is less than 10^{-2} . Top row: piecewise constant functions. Middle row: piecewise linear functions. Bottom row: piecewise quadratic functions.

MHOTV can outperform wavelets regularization in practical applications. Figure 2, for instance, shows fewer spurious oscillations in the MHOTV reconstruction than for Daubechies wavelets penalization. A feature that can also be observed for the 2-D tomographic data. Moreover, our results show that MHOTV regularization requires fewer samples for successful reconstructions than for HOTV and wavelets. Computational efficiency is achieved by performing the transformation in Fourier space or by matrix decomposition, as derived in section 4.1. The associated matlab algorithms can be downloaded at [28], and some of the simulations in the proceeding section can also be found there.

A Proof of Theorem 1

Lemma 1. *Let $k, \ell \in \mathbb{Z}$ with $0 \leq \ell \leq k$. Then we have the following Vandermonde-like identity:*

$$(-1)^p \binom{k}{p} = \sum_{j=0}^{\ell} (-1)^j \binom{k}{j} \binom{k+1}{\ell-j}, \quad (21)$$

where $p = \ell/2$ for ℓ even and $p = (\ell - 1)/2$ for ℓ odd.

Proof of lemma 1. Consider the polynomial $p(x) = (1 - x^2)^k(1 + x)$, which can be factored as $p(x) = (1 - x)^k(1 + x)^{k+1}$. Both representations can be expanded using the binomial sum giving

$$p(x) = \sum_{j=0}^k (-x^2)^j \binom{k}{j} (1 + x) = \sum_{j=0}^k (-1)^j \binom{k}{j} [x^{2j} + x^{2j+1}] \quad (22)$$

by the first representation and

$$p(x) = \left[\sum_{j=0}^k (-x)^j \binom{k}{j} \right] \left[\sum_{j=0}^k x^j \binom{k+1}{j} \right] \quad (23)$$

by the second representation. Since (22) and (23) are equivalent for all x , the coefficients of any particular power of x are equivalent, which is the equality we set out to prove. \square

Proof of theorem 1. Statement 3 is an immediate consequence of statement 2, since each matrix involved in the product is a convolution operator, and convolution operations are commutative and associative.

To prove statement 1, first observe that with increasing m , the nonzero entries in the rows of P_m become increasingly spaced, and it easy to see that the general resulting product P_m^{k+1} is essentially the same for each m with different spacings between the nonzero entries. Thus it is enough to show statement 1 for $m = 1$. In the case $k = 1$, this calculation can be checked directly. So suppose 1 holds for some arbitrary k . Then we need to show that $(P_1 P_1^{k+1})$ yields the desired result as defined by (15). It is fairly easy to see that the resulting entries of this product is simply the addition of two neighboring entries (modulo N) in P_1^{k+1} . Any such entries added together trivially yields the desired values, and the proper location of these values is also easy to confirm.

Similar arguments used for statement 1 also apply to statement 2. First, we can consider an inductive approach, over m , where we will need to show $\Phi_{k,2^{m+1}} = P_{m+1}^{k+1} \Phi_{k,2^m}$. Note that again due to the spacing of the entries of P_m^{k+1} , the argument for any arbitrary m is parallel to that for $m = 1$, with just different handling of the indices. Therefore the case for $m = 1$ suffices for the inductive step, and the case for $m = 1$ is an immediate consequence of the previous lemma. \square

B Definitions

If $f, g \in \mathbb{R}^N$, then the convolution of f and g is given by

$$(f * g)_m = \sum_{n=1}^N f_n g_{m-n}, \quad \text{for } m = 1, 2, \dots, N, \quad (24)$$

where for indices of g running outside of domain of g , a periodic extension of g is assumed. The discrete Fourier transform (DFT) of f is defined by

$$\mathcal{F}(f)_\xi = \sum_{n=1}^N f_n e^{\frac{-i2\pi}{N}(n-1)(\xi-1)} \quad \text{for } \xi = 1, 2, \dots, N, \quad (25)$$

and the inverse discrete Fourier transform (IDFT) of f is given by

$$\mathcal{F}^{-1}(f)_n = \frac{1}{N} \sum_{\xi=1}^N f_\xi e^{\frac{i2\pi}{N}(\xi-1)(n-1)} \quad \text{for } n = 1, 2, \dots, N. \quad (26)$$

Acknowledgements

This work is supported in part by the grants NSF-DMS 1502640, NSF-DMS 1522639 and AFOSR FA9550-15-1-0152.

References

- [1] R. Archibald, A. Gelb, and R. B. Platte. Image reconstruction from undersampled Fourier data using the polynomial annihilation transform. *J. Sci. Comput.*, pages 1–21, 2015.
- [2] G. Beylkin. Wavelets, multiresolution analysis and fast numerical algorithms. *Wavelets Theory and Applications (G. Erlenbacher ao editors), Oxford Univ. Press, New York, Oxford*, 182:262, 1996.
- [3] G. Beylkin, R. Coifman, and V. Rokhlin. Fast wavelet transforms and numerical algorithms i. *Communications on pure and applied mathematics*, 44(2):141–183, 1991.

- [4] S. Bhattacharya, T. Blumensath, B. Mulgrew, and M. Davies. Fast encoding of synthetic aperture radar raw data using compressed sensing. In *2007 IEEE/SP 14th Workshop on Statistical Signal Processing*, pages 448–452. IEEE, 2007.
- [5] P. Blomgren, T. F. Chan, P. Mulet, C.-K. Wong, et al. Total variation image restoration: numerical methods and extensions. In *ICIP (3)*, pages 384–387, 1997.
- [6] K. Bredies, K. Kunisch, and T. Pock. Total generalized variation. *SIAM J. Imaging Sci.*, 3(3):492–526, 2010.
- [7] E. Candès and J. Romberg. Sparsity and incoherence in compressive sampling. *Inverse Probl.*, 23(3):969, 2007.
- [8] E. J. Candès, J. Romberg, and T. Tao. Robust uncertainty principles: Exact signal reconstruction from highly incomplete frequency information. *IEEE Transactions on information theory*, 52(2):489–509, 2006.
- [9] T. Chan, A. Marquina, and P. Mulet. High-order total variation-based image restoration. *SIAM J. Sci. Comput.*, 22(2):503–516, 2000.
- [10] M. A. Cody. The fast wavelet transform: Beyond fourier transforms. *Dr. Dobb’s Journal*, 17(4), 1992.
- [11] R. R. Coifman and D. L. Donoho. *Translation-invariant de-noising*. Springer, 1995.
- [12] I. Daubechies et al. *Ten lectures on wavelets*, volume 61. SIAM, 1992.
- [13] M. Eck, T. DeRose, T. Duchamp, H. Hoppe, M. Lounsbery, and W. Stuetzle. Multiresolution analysis of arbitrary meshes. In *Proceedings of the 22nd annual conference on Computer graphics and interactive techniques*, pages 173–182. ACM, 1995.
- [14] Y. C. Eldar and G. Kutyniok. *Compressed sensing: theory and applications*. Cambridge University Press, 2012.
- [15] H.-Y. Gao. Wavelet shrinkage denoising using the non-negative garrote. *Journal of Computational and Graphical Statistics*, 7(4):469–488, 1998.
- [16] T. Goldstein and S. Osher. The split Bregman method for l1-regularized problems. *SIAM J. Imaging Sci.*, 2(2):323–343, 2009.
- [17] K. Guo and D. Labate. Optimally sparse multidimensional representation using shearlets. *SIAM journal on mathematical analysis*, 39(1):298–318, 2007.
- [18] U. Kamilov, E. Bostan, and M. Unser. Wavelet shrinkage with consistent cycle spinning generalizes total variation denoising. *IEEE Signal Processing Letters*, 19(4):187–190, 2012.
- [19] G. Kutyniok et al. *Shearlets: Multiscale analysis for multivariate data*. Springer Science & Business Media, 2012.

- [20] R. Leary, Z. Saghi, P. A. Midgley, and D. J. Holland. Compressed sensing electron tomography. *Ultramicroscopy*, 131:70 – 91, 2013.
- [21] C. Li, W. Yin, H. Jiang, and Y. Zhang. An efficient augmented lagrangian method with applications to total variation minimization. *Comput. Optim. Appl.*, 56(3):507–530, 2013.
- [22] M. Lustig, D. Donoho, and J. M. Pauly. Sparse mri: The application of compressed sensing for rapid mr imaging. *Magnetic resonance in medicine*, 58(6):1182–1195, 2007.
- [23] M. Lysaker, A. Lundervold, and X.-C. Tai. Noise removal using fourth-order partial differential equation with applications to medical magnetic resonance images in space and time. *IEEE Transactions on Image Processing*, 12(12):1579–1590, Dec 2003.
- [24] S. Ma, W. Yin, Y. Zhang, and A. Chakraborty. An efficient algorithm for compressed MR imaging using total variation and wavelets. In *Computer Vision and Pattern Recognition, 2008. CVPR 2008. IEEE Conference on*, pages 1–8, June 2008.
- [25] S. Mallat. *A wavelet tour of signal processing: the sparse way*, pages 292–296. Academic press, 2008.
- [26] F. Natterer. *The Mathematics of Computerized Tomography*. Society for Industrial and Applied Mathematics, 2001.
- [27] L. I. Rudin, S. Osher, and E. Fatemi. Nonlinear total variation based noise removal algorithms. *Physica D: Nonlinear Phenomena*, 60(1):259–268, 1992.
- [28] T. Sanders. Matlab imaging algorithms: Image reconstruction, restoration, and alignment, with a focus in tomography. <http://www.toby-sanders.com/software>, <https://doi.org/10.13140/RG.2.2.33492.60801>. Accessed: 2016-19-08.
- [29] T. Sanders. *Image Processing and 3-D Reconstruction in Tomography*. PhD thesis, University of South Carolina, 2015. Chapter 1: Background.
- [30] T. Sanders. Parameter Selection for HOTV Regularization. *ArXiv e-prints*, Aug. 2016.
- [31] T. Sanders, A. Gelb, R. Platte, I. Arslan, and K. Landskron. Recovering fine details from under-resolved electron tomography data using higher order total variation regularization. *Ultramicroscopy*, 174:97–105, 2017.
- [32] J.-L. Starck, F. Murtagh, and J. M. Fadili. *Sparse image and signal processing: wavelets, curvelets, morphological diversity*. Cambridge university press, 2010.
- [33] W. Stefan, R. A. Renaut, and A. Gelb. Improved total variation-type regularization using higher order edge detectors. *SIAM J. Imaging Sci.*, 3(2):232–251, 2010.
- [34] G. Steidl and J. Weickert. Relations between soft wavelet shrinkage and total variation denoising. In *Joint Pattern Recognition Symposium*, pages 198–205. Springer, 2002.

- [35] G. Steidl, J. Weickert, T. Brox, P. Mrázek, and M. Welk. On the equivalence of soft wavelet shrinkage, total variation diffusion, total variation regularization, and sides. *SIAM Journal on Numerical Analysis*, 42(2):686–713, 2004.
- [36] C. Taswell. The what, how, and why of wavelet shrinkage denoising. *Computing in science & engineering*, 2(3):12–19, 2000.
- [37] A. Temizel, T. Vlachos, and W. Visioprime. Wavelet domain image resolution enhancement using cycle-spinning. *Electronics Letters*, 41(3):119–121, 2005.
- [38] F. C. Tenoudji. Wavelets; multiresolution analysis. In *Analog and Digital Signal Analysis*, pages 337–373. Springer, 2016.
- [39] Y. Wang, J. Yang, W. Yin, and Y. Zhang. A new alternating minimization algorithm for total variation image reconstruction. *SIAM J. Imaging Sci.*, 1(3):248–272, 2008.
- [40] S.-J. Wei, X.-L. Zhang, J. Shi, and G. Xiang. Sparse reconstruction for sar imaging based on compressed sensing. *Progress In Electromagnetics Research*, 109:63–81, 2010.